Graduate School ETD Form 9
(Revised 12/07)

PURDUE UNIVERSITY
GRADUATE SCHOOL
Thesis/Dissertation Acceptance

This is to certify that the thesis/dissertation prepared

By Zachary Ryan Bart

Entitled
Multi-scale Analysis of Morphology, Mechanics, and Composition of Collagen in Murine Osteogenesis Imperfecta

For the degree of Master of Science in Biomedical Engineering

Is approved by the final examining committee:

Joseph Wallace
Chair

Hiroki Yokota

Sungsoo Na

To the best of my knowledge and as understood by the student in the *Research Integrity and Copyright Disclaimer (Graduate School Form 20)*, this thesis/dissertation adheres to the provisions of Purdue University's "Policy on Integrity in Research" and the use of copyrighted material.

Approved by Major Professor(s): Joseph Wallace

Approved by: John Schild 07/11/2013
Head of the Graduate Program Date

MULTI-SCALE ANALYSIS OF MORPHOLOGY, MECHANICS, AND COMPOSITION OF COLLAGEN IN MURINE OSTEOGENESIS IMPERFECTA

A Thesis
Submitted to the Faculty
of
Purdue University
by
Zachary Ryan Bart

In Partial Fulfillment of the
Requirements for the Degree
of
Master of Science in Biomedical Engineering

August 2013
Purdue University
Indianapolis, Indiana

ACKNOWLEDGEMENTS

I would like to express my gratitude to my thesis advisor, Dr. Joseph Wallace, for his insight, guidance, and support over the last two years. The research opportunity he provided to me as well as the ideas he shared with me have taught me several useful and interesting techniques.

Furthermore, I would like thank the members of my advisory committee, Dr. Hiroki Yakota and Dr. Sungsoo Na. Their graduate courses proved to be very engaging and useful for understanding topics from new angles.

Additionally, I would like to thank all of my research colleagues: Mr. Max Hammond, Ms. Silvia Canelón, Mr. Armando Diaz-Gonzalez, Mr. Terrill Richardson, and Mr. James Holman. They have all provided significant help, and their personalities made the lab environment enjoyable. I would also like to thank Dr. Edward Berbari and Dr. John Schild for the teaching opportunities they provided to me prior to beginning my research work. Finally, I want to thank my brother, Adam, and my friends. Their support has helped me cope with some of the more difficult moments I have faced in the last few years.

TABLE OF CONTENTS

Page

Page

LIST OF TABLES

LIST OF FIGURES

Figure Page

Figure Page

LIST OF ABBREVIATIONS

Symbol	Description
AFM	Atomic Force Microscopy
CaHA	Hydroxyapatite, Pure crystal
$Ca_{10}(PO_4)_6(OH)_2$	Hydroxyapatite, Body crystal
CDF	Cumulative distribution function
CH_2	Methylene
CO_3^{2-}	Carbonate
Col1α1	Collagen Type I, alpha-1 gene, or associated protein
Colα2	Collagen Type I, alpha-2 gene, or associated protein
EDTA	Ethylenediaminetetraacetic Acid
FWHM	Full-width half max
G349→C	349^{th} Amino acid has a cysteine substituting for a glycine
μCT	Micro Computed Tomography
oim	Osteogenesis imperfecta murine
oim/oim	Homozygous form of osteogenesis imperfects murine animal
oim/+	Heterozygous form of osteogenesis imperfecta murine animal
PO_4^{3-}	Phosphate
RPI	Reference Point Indentation
WT	Wild Type

NOMENCLATURE

Symbol	Unit	Description
D	nm	Periodic D-spacing of collagen fibril
MMR		Mineral to Matrix Ratio
ID	µm	Indentation distance
IDI	µm	Indentation distance increase
TID	µm	Total indentation distance
CID	µm	Creep indentation distance
vBMD	g/cm^3	Volumetric bone mineral density
BV/TV		Bone volume to tissue volume ratio

ABSTRACT

Bart, Zachary Ryan. M.S.B.M.E., Purdue University, August 2013. Multi-Scale Analysis of Morphology, Mechanics, and Composition of Collagen in Murine Osteogenesis Imperfecta. Major Professor: Joseph Wallace.

Osteogenesis imperfecta is a rare congenital disease commonly characterized by brittle bones caused by mutations in the genes encoding Type I collagen, the single most abundant protein produced by the body. The murine model (oim) exists as a natural mutation of this protein, converting its heterotrimeric structure of two Col1a1 molecules and a single Col1a2 molecule into homotrimers composed of only the former. This defect impacts bone mechanical integrity, greatly weakening their structure.

Femurs from male wild type (WT), heterozygous (oim/+), and homozygous (oim/oim) mice, all at 12 weeks of age, were assessed using assays at multiple length scales with minimal sample processing to ensure a near-physiological state. Atomic force microscopy (AFM) demonstrated detectable differences in the organization of collagen at the nanometer scale that may partially attribute to alterations in material and structural behavior obtained through mechanical testing and reference point indentation (RPI). Changes in geometric and chemical structure through the use of μ-Computed Tomography and Raman spectroscopy respectively indicate a smaller, brittle phenotype caused by oim. Changes within the periodic D-spacing of collagen point towards a reduced mineral nucleation site, supported by reduced mineral crystallinity, resulting in altered material and structural behavior in oim/oim mice. Multi-scale analyses of this nature offer much in assessing how molecular changes can compound to create a degraded, brittle phenotype.

1. OVERVIEW

1.1 Hierarchical Structure of Bone

Bones within the body are complex organ structures that fill several vital purposes. Firstly, larger bone structures act as protection for the major vital organs found within the torso and the head. The ribcage and the skull protect the lungs, heart, and brain from external trauma. Aside from protection, bones provide support and form to the remainder of the body. This form allows for various locations within the body to attach muscles, allowing locomotion to occur through pulling these lever-like bones within major extremities. Apart from mechanics and protection, bones also serve the important purpose of manufacturing red blood cells for the body. The mineral composition of bone also allows for the storage and distribution of ions used by other body systems, creating mineral ion homeostasis. For instance, calcium is an integral molecule for signaling in the nervous system. In the case where an individual does not intake enough calcium, the body will actually resorb away some of its bone to obtain the calcium ions it needs to function properly.

In order to understand bone as a material, it is important to understand that it exists as a hierarchical structure. Each level of bone's organization is affected by the arrangement of its smaller constituents, and the different levels are unique from one another. At the organ level, each bone in the skeleton has a shape that reflects its purpose. The femur and tibia of the leg are long, slender bones that act as levers for movement, while the flat, curved bones of the skull form an enclosure to protect the brain. These structures are made up of multiple types of bone material that serve different purposes within the bones themselves.

Considering just one of the long bones, simple radiographs can begin to show deeper levels of organization. A breakdown of the hierarchical structure can be seen in figure 1.1. Single bones are comprised of two types of tissue structures, cortical and cancellous bone. While these types of tissue are composed of the same mineralized material, their organizational differences point to their functions. Cancellous, or trabecular bone, is found at the end of long bones, and forms as a porous web-like structure (80-85% porosity) [1]. This structure acts as a shock-absorber to better cushion bones from rigorous activities. This porous region is also where much of red blood cell production occurs. This region contains red bone marrow, a tissue rich in hematopoietic stem cells that are the precursors to most blood cells. In contrast, cortical, or compact bone is a very dense structure. This bone type forms the hard shell of bone that most people are more familiar with. This formation provides the primary structural stability of the bone and is thus denser (2-5% porosity) than the previously mentioned trabecular regions.

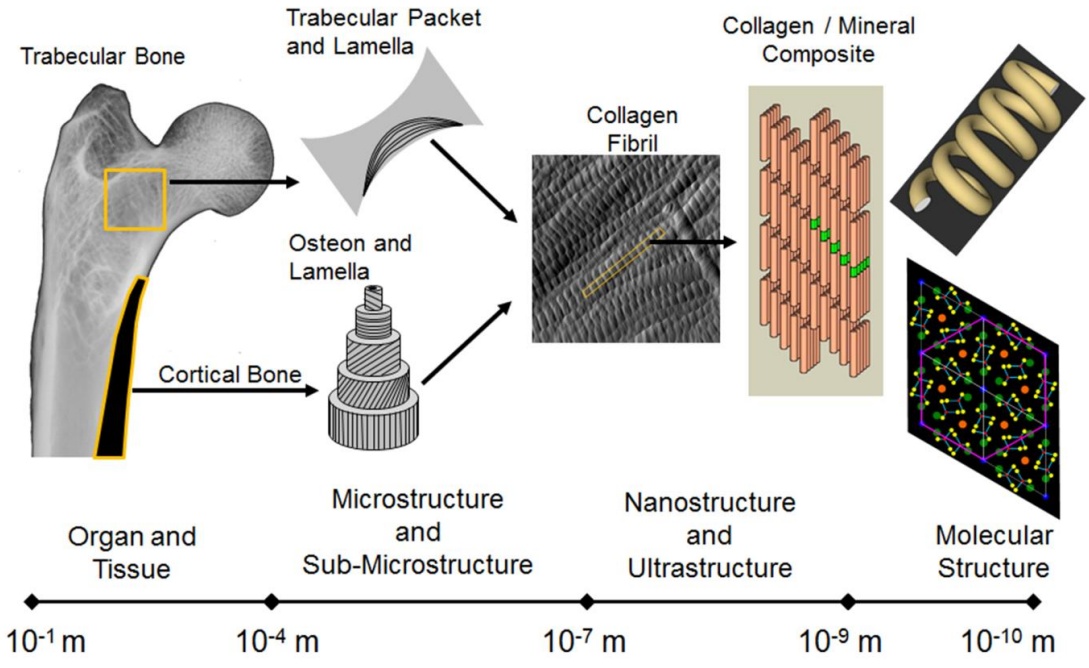

Figure 1.1: Overall hierarchical structure of bone [2]. It can be seen that at each length scale the organizational patterns vary greatly.

While cancellous and cortical bone are made from the same base materials, the structure that forms the web and shell arise from different organizational patterns. Mature cortical bone is primarily created in what is called an osteon structure. A cross-section of an osteon shows a ring-like pattern centered on a single Haversian canal that contains blood vessels involved in providing nutrition to cells residing within the mineral matrix (Figure 1.2A). These cells, osteocytes, arise as a byproduct of the primary formation and remodeling of bone. A portion of bone-forming cells, osteoblasts, become entrapped in the mineral matrix and create a connected network of bone cells. Comparatively, trabecular packets that form the webbing at the ends of bones (Figure 1.2B) have few osteocytes embedded, forming a structure with fewer cells inside the mineralized material [3-5].

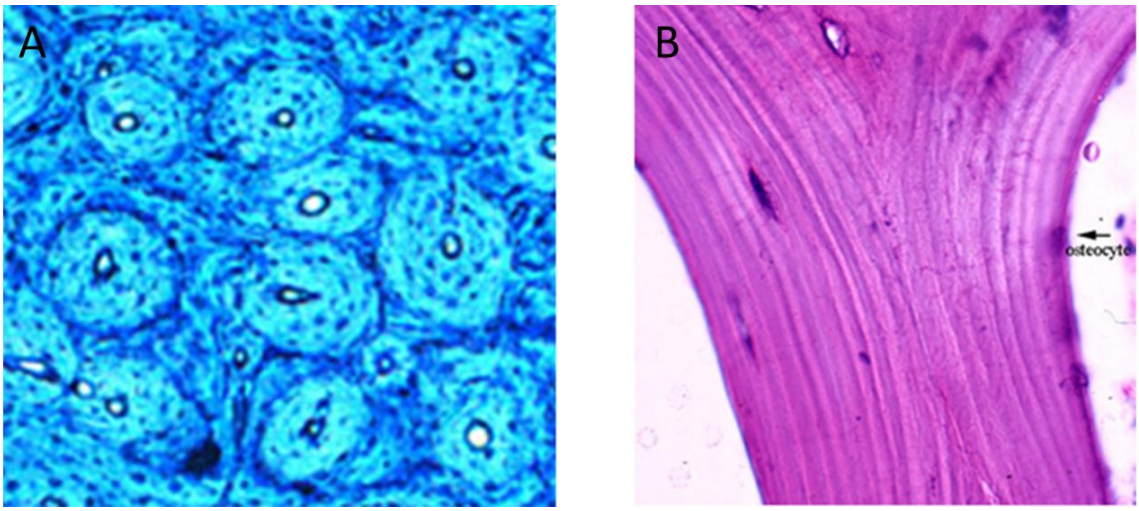

Figure 1.2: Histology of bone types. (A) Toluidine blue stained cross-section of osteon structures. (B) Hematoxylin and eosin stained section of single trabeculae. The primary difference can be seen with the amount of osteocytes that are embedded in the osteon system compared to the trabecular packet. Images courtesy of Joseph Wallace.

Apart from the cellular network contained in the bone structures described above, the areas between osteocytes is comprised of the mineralized tissue most commonly associated with bone. This mineralized matrix is responsible for creating bone rigidity and provides storage for the body's dietary minerals. This mineralized matrix is also a

complex, composite material. Approximately two-thirds of bone's weight is created by inorganic hydroxyapatite, $Ca_{10}(PO_4)_6(OH)_2$. This mineral forms as a hexagonal crystal, roughly 2-3 nm in length, 25 nm in width, and 50 nm in length [6]. While this crystal lattice is the ideal form of hydroxyapatite, human diet may cause ions like magnesium, strontium, sodium, potassium, and carbonate to substitute for some of the chemical structure. The remaining one-third constitutes the organic material found in bone. Of this organic material, roughly 10% of it is comprised of other cells, lipids, and growth factors. The majority of this organic matter is comprised of a single protein, Type I collagen.

1.2 Type I Collagen in Bone

Collagen is the single most abundant protein found in the body [7]. All 29 types of collagen account for roughly 25-35% of the total protein content in the body, and exist as similar proteins with different polypeptide sequences. These proteins have different structures. For instance, some are fibrillar in nature, while others are not. Of this content, Type I collagen is the most common variety, accounting for 90% of the total collagen content [8]. Type I collagen, similar to bone, follows a complex hierarchical structure. At the single protein scale, Type I collagen is comprised of a unique heterotrimeric, triple helical structure. This right-handed triple helix is created as a combination of two Col1α1 molecules, and a single Col1α2 molecule. While these two types of molecules are different, they share a common repeating amino acid motif [Glycine – X – Y], where glycine is repeated every third amino acid in the chain. Glycine plays a key role in developing the triple helix structure. As the simplest amino acid, with only a single hydrogen as its side-chain, the triple helix forms in such a way that the individual glycine molecules fill the vacant space formed by the helical pattern [9]. X and Y represent many different amino acids, most commonly proline and hydroxyproline. The difference in this X – Y sequence confers the difference between the Colα1 and Colα2 molecules.

Collagen molecules arrange themselves in a unique way. Some of the earliest X-Ray diffraction imaging of collagen microfibrils revealed a unique banding pattern

associated with Type I collagen [10]. While early images were of poor resolution, it could be seen that the banding structure, later called the D-periodicity or D-spacing, had a fixed width of approximately 67 nm. Recent studies using more refined imaging techniques have confirmed this approximation, but have shown that this banding exists as a distribution near this value, with potential alterations linked with disease states [11-13].

Initially, this banded structure of collagen was not fully understood. Through the imaging of single tropocollagen molecule strands [14], it was discovered that a single molecule had a length equal to 4.4 times the 67 nm banded repeat distance found in aggregated fibrils. This finding implied that there must be some overlap between adjacent molecules in this aggregate equal to 0.4 times the repeated distance. This overlapping period then creates a staggered array of molecules in what came to be known as the collagen microfibril. Drawing out all the possible arrangements of this staggered array, Hodge and Petruska showed that the molecules could not exist in direct contact with neighboring molecules in a given row, giving rise to a gap region equal to 0.6 times the D-spacing. As larger aggregates form, it can be seen from Figure 1.3 that this gap-overlap design will create regions where collagen molecules are aligned/continuous in adjacent row, while there is another region where the gaps occur. These differences in tropocollagen alignment lead to the banded structure seen in earlier imaging studies.

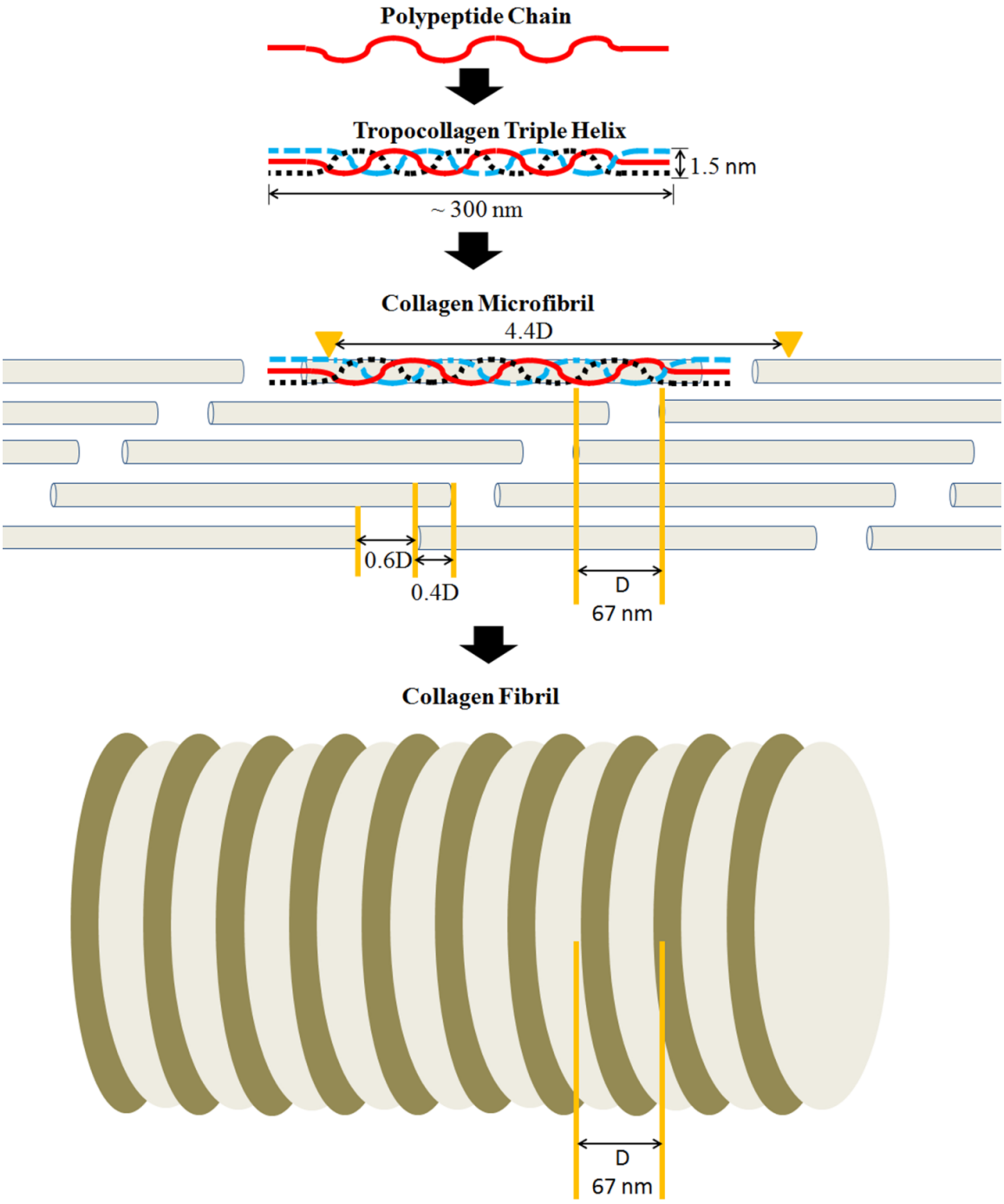

Figure 1.3: Hierarchical development of a collagen fibril. 300 nm long tropocollagen molecules form together in a staggered array, ultimately creating a repeated banding pattern seen in fibrils measuring 67 nm. This 67 nm distance, D, is formed by tropocollagen molecules overlapping a distance equal to 0.4D and a gap region equal to 0.6D.

While this gap distance was initially defined in the model out of mathematical necessity, pores within collagen had been observed in earlier studies [15]. Regardless, this 2 dimensional model of a parallel, staggered array of tropocollagen molecules fails to explain how a 3 dimensional fibril with a periodic D-spacing structure forms. More recent three-dimensional models of collagen based on electron density maps developed from X-Ray diffraction data [16] follow this early model very closely. These models validated older models of type I collagen in a three-dimensional space.

Despite being theorized first to justify a model of collagen, a 40 nm gap region may play an important role in bone mineralizaiton. Current theories of the mineralization process of bone point to these gap regions between tropocollagen molecules serving as an origin site for the hydroxyapatite crystal [17]. The 40 nm spacing is serviceably large enough to act as a nucleation site for mineralization. The spaces are also filled with the telopeptides of collagen molecule strands, creating a negatively charged region [18] that further stimulates the nucleation process. This mineral then grows along the collagen microfibrils and forms the base composite material that develops into a single layer of bone. These single layers of bone then stack in various directions to form a material that is resistant to deformation in directions associated with naturally occurring loads. While this mineralization process is still debated, the development of mineralized tissue is tightly regulated. Alterations to either the organic matrix or the mineral crystals that are not repaired by bone remodeling can lead to structural deformities that can damage the overall skeletal structure.

1.3 Collagen and Skeletal Diseases

Since type I collagen is the most common protein in the body, damage to its production can produce dire consequences. Similarly, arrested skeletal development can greatly damage an individual's quality of life, or result in premature or prenatal death. Many different bone diseases exist, and several find their roots in defective collagen. The most commonly known degenerative bone disorder, osteoporosis, leads to an overall drop

in bone quality, greatly increasing risk of severe fractures. Other diseases, like scurvy or Ehler's-Danlos syndrome, act on the collagen that creates bone, skin, and cartilage, leading to weaker bones and the deformation of other collagen-containing connective tissues.

The most notable of these collagen-affecting diseases is Osteogenesis Imperfecta (OI). OI is a genetic disease that affects a portion of either some or both of the Col1α1 and Col1α2 genes through glycine substitutions or alterations to protein splice sites [19]. As a disease, OI has a spectrum of severities. The severity can be based on the location of the mutation, or the number of mutations. Mutations located nearer the C-terminus of the protein slow the formation of the triple helix, allowing for more post-translational modifications the individual protein strands. Additionally, severity is dependent on if one or both genes are affected. In the case where only one gene is affected, it is still possible for the body to produce normal collagen molecules.

Typically, OI develops as a genetic modification that causes substitutions of glycine molecules with larger amino acids within the tropocollagen molecules [19]. Specific variants of the disease denote different symptom levels, but they all manifest with some reduction in bone quality or quantity, leading to greatly increased bone fracture risk. This has given OI the moniker "brittle bone" disease. Currently, there are four main types of the disease, referred to as Sillence classifications [20]. Additional classifications five through eight have been added more recently. The four main types suffer from additive complications of insufficient collagen quantity and reduced collagen quality. Type II OI suffers from both of these collagen deficiencies and is typically fatal within the first year after birth. Comparatively, Type I (Quality normal, quantity low) patients suffer brittle bones, reduced muscular development, and a blue coloring of sclera that is often indicative of this type of OI. In the opposite case, Type III (Quality low, quantity normal), patients still experience some of the same symptoms as Type I, but will also exhibit severe bone deformation and typically have a much smaller stature. This disease is only a mutation of the collagen protein, yet it demonstrates the clear link

between the organic and mineral portions of bone. Due to this fact, models of this disease offer much in understanding how the organic and inorganic phases of bone interact with one another.

Implications of this disease point to the fact that molecular changes of collagen will alter material and structural properties not only of the whole bone, but potentially at every length scale. This link has led to several different collagen-deficient animal models being developed. For instance, BrtlIV is a mouse model that has been genetically engineered to replace a single glycine molecule with a cysteine (G349→C) in the Col1α1 chain, creating a brittle phenotype [21]. An older model, Mov-13, has one or both Col1α1 rendered null by genetic insertion [22]. The latter case of Mov-13 is always prenatally fatal due to collagen forming from only Colα2 molecules. However, the genetically heterozygous Mov-13 animal produces a normal amount of collagen in reduced quality, mimicking the effect of Type I OI.

Apart from genetically engineered model, there is one naturally occurring mutation that has been discovered, the osteogenesis imperfecta murine, or oim model. Animals of this strain have a random mutation that has inactivated one or both of the genes responsible for the creation of the Col1α2 strand of type I collagen [23]. This mutation leads to a model of mild to severe type III OI based on the inactivation of one or both genes. In the homozygous case, the mouse is incapable of creating proper tropocollagen molecules, leading to the creation of Type I collagen solely from α1 helices. Collagen made in this fashion possess altered structures has shown to be weaker [24], create smaller tendons [25], and have a larger intermolecular spacing [26]. The heterozygous animal has shown to create a phenotype similar to a less severe state of this disease [27]. This disease is not limited to affecting bone and tendon. Any tissue containing Type I collagen, like teeth or muscle have also shown reduced mechanical ability caused by homotrimer substitutions [28, 29]. Studies contained within this body of work are focused on analyzing this oim model of OI.

1.4 Analysis Assays

Analysis of genetic disease is typically best done at a scale as near the mutation as possible. This creates an observation point closer to the root cause of the disease, not behind the cascade of complications. It is also important to characterize the phenotype at other levels to see how mutations can manifest into higher level alterations. In the case of the oim model, a genetic mutation of tropocollagen has influences on all levels of bone organization. Due to this fact, this disease model would be best studied at as many organizational levels as possible. Techniques described in this section allow for multi-scale analysis of the oim phenotype to be measured with minimal sample processing. Excessive processing, like dehydration or sample powdering is avoided in order to ensure that samples are as close to physiological state as possible. Only the first assay described in this chapter required polishing and light demineralization of samples to expose measurable collagen. All other assays were accomplished using hydrated, unprocessed tissues. While this chapter will serve as a brief overview of the techniques, specific information of how these techniques were applied can be found in the Materials & Methods section.

The first technique used in this study is atomic force microscopy (AFM). AFM imaging provides structural information of collagen at the nano-scale. This technique allows for a direct measure of the periodic D-spacing associated with the collagen fibril structure. This is done by scanning a sharp probe attached to a silicon cantilever across a surface. Differences along the surface topology of collagen fibrils will cause the cantilever to deflect. When this deflection is detected by the control system, the stage holding the sample is adjusted up or down by piezoelectric transducers some amount to restore the cantilever to its “setpoint” position. This movement of the stage is recorded and creates a Z-scale intensity image of the collagen surface that can be used to analyze the D-spacing of single collagen microfibrils.

Apart from collagen analysis at the nano-scale, it is also useful to perform measures of the mineral phase at small length levels. Raman spectroscopy provides

quantitative information on both the mineral and the organic phase of bone. This gives information about the nano-structure, but averaged over a micro-scale area. Raman spectroscopy is known as a vibrational spectroscopy (Figure 1.4). A single laser is focused on the surface of a specimen, with some of the energy penetrating some distance into the surface. This energy causes molecular bonds to vibrate, causing a shift in the light energy reflected back and measured by the detector of the Raman system. This Raman shift is unique to given substances, created by the change in wavelength of the reflected light. A general spectrum is not actually created by the content of molecules within a compound, but by the bonds between molecules. For instance, the Raman spectrum of graphite is inherently different from that of diamond despite both being entirely carbon atoms. The Raman spectrum of bone has been studied thoroughly in the past [30-32], so changes detected by this technique can be used to identify alteration in the material.

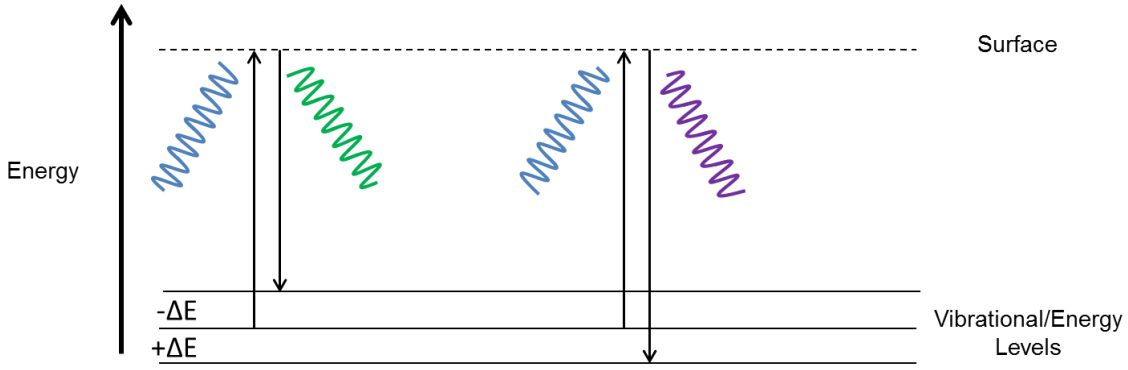

Figure 1.4: Schematic of Raman spectroscopy. A laser is shined on a surface, vibrating the chemical bonds of the material. In this case, the initial laser (blue) is of a known wavelength. There are two possibilities. In the first, the material absorbs some of the energy, causing an upward shift (green) of the wavelength. In the second case, the vibration of molecules causes the material to release energy, sending back a higher energy, lower wavelength (violet).

As technology has developed, new techniques have been created to provide useful information in a clinical setting. Reference Point Indentation (RPI) provides information similar to what is obtained from traditional mechanical testing with minimal damage induced to the structure. RPI uses a dual probe array to assess the material structure. A

reference probe is placed on the surface of the bone while an indentation probe is extended from inside of the reference probe into the bone. This indentation process is cycled a number of times, creating data over a number of cycles. While this process does induce some damage to the surface of the bone, damage is only locally isolated to a 100 μm area [33]. Measures taken from indentation have been linked to material modulus and creep behavior. RPI promises clinical relevance. One design of the reference probe (not shown in the figure) is that of a hypodermic needle, providing a means to take transcutaneous measures of bone [34]. Studies involving RPI with humans have shown differences in mechanical behavior with osteoporotic fractures as well as showed RPI's potential as a clinical technique capable of detecting fractures.

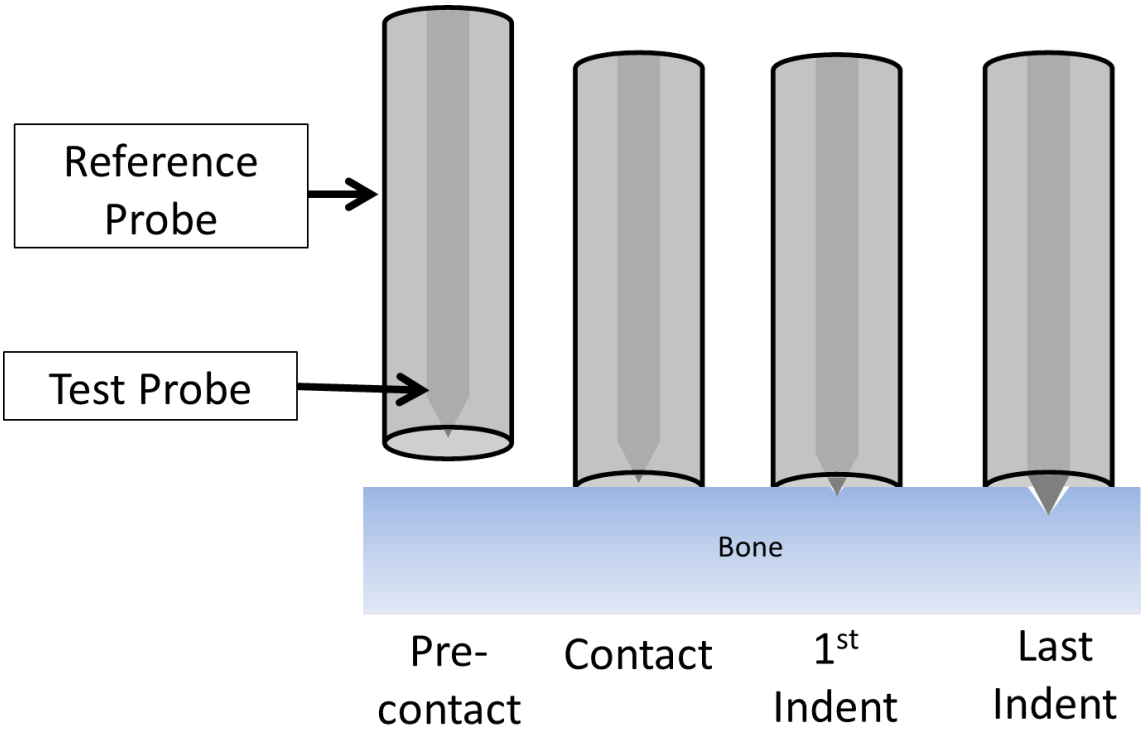

Figure 1.5: Schematic representation of reference point indentation (RPI). A reference probe is lowered into contact with the material in question. After this, a load-sensitive probe inside the reference probe is used to indent the surface a number of times to create mechanical data. Image courtesy of Max Hammond.

Another common imaging technique used to study bone is microcomputed tomography (μCT). In its most basic form, μCT creates three-dimensional images of bones through the use of serial X-ray images taken by rotating a sample. More advanced μCT systems are capable of measuring the cortical and trabecular structure of bones down to the sub-μm level. More information on this technique and its use in studying bone can be seen in a review article I have awaiting publication in Advances in Computed Tomography entitled "Microcomputed Tomography Applications in Bone and Mineral Research."

As stated earlier, traditional mechanical testing provides a good deal of useful information about the structural and material properties of bone. Three-point bending of bones provides material information like elastic modulus and toughness, and structural information like stiffness. Both of these types of measures provide useful information. Material alterations caused by disease point to an alteration in bone's constituents, while structural weaknesses are convoluted by bone deformation associated with this disease. While inherently destructive, three-point bending, as is the case with all previous tests, can be done at near physiological conditions if a bone is kept in a hydrated state. The main weaknesses associated with these tests are the limitations from the assumptions required to utilize small deformation equations. Because of this, interpretation of data taken from gross mechanical testing is most reliable at small strains. While these equations have some limitations, measures of the plastic deformation region still hold useful information in understanding how bone performs under higher load levels.

2. INTRODUCTION

Bone is a complex material, with levels of structural organization that exist over several orders of magnitude in length scale [35]. At the whole bone level, cortical bone forms a rigid shell to support the major loading the bone encounters, while trabecular webbing at the ends of the bone acts to protect the bone through h its shock-absorbing ability [36]. At smaller length scales in cortical bone are osteons, a network of connected cells called osteocytes in concentric ring-like structures. Each ring is composed of lamellae which, themselves, are built from collagen fibrils seeded with inorganic hydroxyapatite crystals. This collagen/mineral composite is the base constituent that crafts bone as a tissue and material. Understanding bone from a material standpoint is an inherently difficult task. While imaging can provide insight into material architecture and organization, this alone is not enough to understand how that material functions at the structural level. Mechanical testing can be used to assess the strength of the bone as a structure, but it must be coupled with some form of imaging to estimate material properties of the bone [37]. Together, these methods are useful for assessing whole bone qualities and for estimating tissue level behavior, but they do little to shed light on problems which may exist at smaller length scales (i.e. disease induced changes to the fundamental constituents of the tissue).

The fundamental constituents of bone, Type I collagen and hydroxyapatite, have been well characterized and their composition is well known [26, 38, 39]. Hydroxyapatite crystals are created from calcium, phosphate, and hydroxide, with various potential substitutions for these ions (e.g. carbonate or fluoride). Collagen fibrils typically do not have these types of substitutions. At the molecular level, a single collagen alpha helix has a repeating triplet motif of a glycine molecule, followed by two other amino acids. These

two others are often proline or hydroxyproline, which causes many to assess collagen content by the amount of hydroxyproline [40]. Glycine's presence as every third amino acid is highly important in this structure as well. Since its R-chain is a single hydrogen atom, this allows for the glycine to be tucked along the axis of the helix shape made by the molecules [9]. These collagen molecules then aggregate to form larger structures, the collagen fibril.

Collagen fibrils are made from hundreds of triple helical tropocollagen molecules coming together to form a 3 dimensional fibrillar pattern [16]. These heterotrimeric triple helices are created as a mixture of two α1 molecules and one α2 molecule. These α chains are both created with the same type of repeating structure described above, but are unique from one another in their specific amino acid sequence. Differences in the amino acid chains, especially molecules like lysine, dictate where cross-linking will occur between the α1 and α2 molecules. These triple helices stack upon themselves in a staggered, repeating fashion, creating gaps at the end of each tropocollagen molecule within a row. Due to this staggered-gap structure (Figure 2.1), there is a repeated pattern where tropocollagen molecules overlap adjacent to a region where one tropocollagen gap exists. This overlap-gap repeating structure has been shown to have a fixed periodic repeat distance, the 67 nm D-periodicity [14]. However, recent studies have shown that this D-spacing exists as a distribution of values which varies as a function of several disease states including osteoporosis [12], Osteogenesis imperfecta [11], and simply in different collagen-based tissues[41]. Since collagen and mineral are the basic building materials of bone, understanding how they interact to build larger structures is key to assessing bone in a material sense.

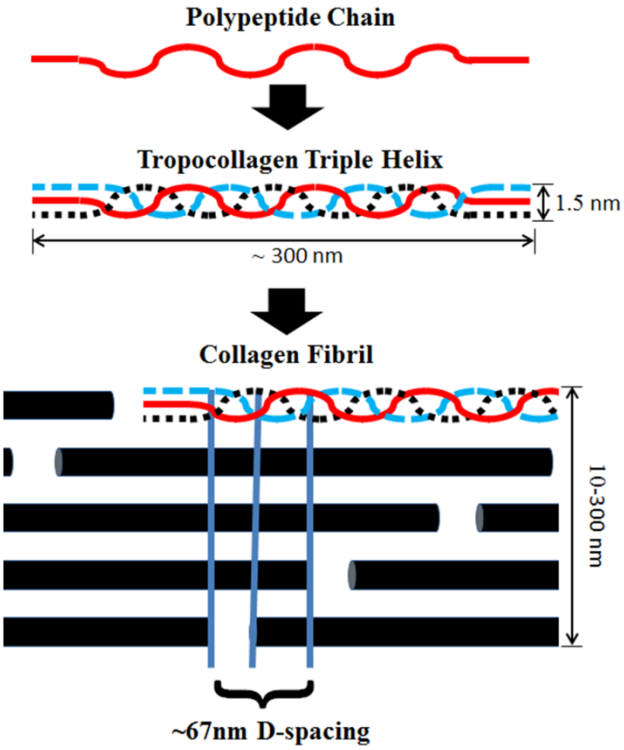

Figure 2.1: The basic formation of collagen fibril structure. The tropocollagen triple helix is formed from 2 α1 molecules and 1 α2 molecule to create a heterotrimer structure. These tropocollagen molecules stack in a staggered fashion, creating a gap-ridge repeating structure. This period associated with this repeating structure is approximately 67nm [14].

Osteogenesis imperfecta (OI) is a rare congenital disease of collagen wherein the triple helix of collagen is compromised due to mutations in either the α1 or α2 collagen chains [20]. These mutations lead to defective collagen fibrils in collagen-based tissues including bone, skin and dentin [42]. The dominant OI phenotype is in bone and involves fracture due to reduced bone quality, leading to the term "brittle bone" disease. A murine model (OIM), discovered through random mutations, has a phenotype similar to a mild to severe Type III OI in humans [23]. This model is driven by a recessive mutation in the gene encoding the α2 chain. In the homozygous case (oim/oim), all Type-I collagen molecules and fibrils within the animal are created as homotrimers of α1 chains. These homotrimers have different cross-linking of polypeptide molecules [43]. In the case of the heterozygous mouse (oim/+), the animal can still produce some measure of normal α2

chains. As such, there is a mixture of both normal heterotrimeric molecules as well as molecules containing homotrimeric triple helices. A combination of homotrimers and heterotrimers are then incorporated into fibrils. This mutation alone has been shown to greatly reduce the mechanical properties of bone [27].

Many studies in oim mice have been performed over the past 20 years, assessing how this change in molecular collagen alters higher level properties. These studies have shown reduced mineral crystallinity [24] , altered fatigue response [44], reduced bone size [45], and more brittle mechanical and structural properties [45, 46]. Further studies have attempted to find ways to mitigate the damage done by the disease state [47, 48], and how it is affected by common treatments for bone disorders [49, 50]. A limitation of previous oim investigations is that most assays are performed at one or two discrete length scale. As bone is a composite material with varying organization at each level of the structural hierarchy, it is important to approach the analysis of bone at multiple levels ranging from the nanoscale to the whole bone to understand how nanoscale changes impact each level of organization. Furthermore, maintaining samples as close to a physiological state as possible through hydration and minimal processing is important to minimize artifacts that can arise during processing (i.e. dehydration, embedding, etc.). The goal of this study was to perform a multi-scale phenotypic analysis of bone from heterozygous and homozygous oim mice, maintaining samples as close to physiological conditions as possible. It was hypothesized that the underlying issue associated with this disease is linked to a problem with the ability to properly form and organize the collagen matrix. This alteration of the organic matrix may impact the formation and performance of the inorganic phase of bone.

3. MATERIALS AND METHODS

3.1 Animals

Animals were obtained from The Jackson Laboratory at approximately 12 weeks of age. All animal handling was done with prior IACUC approval (protocol number SC197R).Thirty-five female mice from 3 groups were utilized: homozygous; B6C3Fe a/a-Col1a2^{oim}/Col1a2^{oim} (oim/oim, n = 11), heterozygous; B6C3Fe a/a=Col1a2^{oim}/J (oim/+, n = 9), and wild type control; B6C3FeF1/J a/a (WT, n = 15). Sample sizes between groups were different due to *in vivo* fractures and/or deaths in the oim/oim group caused by the disease state, as well as shipping errors resulting in a portion of the oim/+ group arriving at 13 weeks of age. Upon arrival at 12 weeks of age, animals were sacrificed via CO_2 inhalation, at which time animals were weighed, and then femora were harvested, stripped of soft tissue and stored wrapped in phosphate buffered saline (PBS) soaked gauze at -20 °C.

3.2 Atomic Force Microscopy (AFM)

Right femora (n = 5 per group) were processed and imaged using atomic force microscopy (AFM) as previously described [13]. Each bone had distal and proximal ends removed with a low-speed sectioning saw. Bones were then mounted to a steel disk with anterior side facing up, using cyanoacrylate glue. A flat surface along the anterior side was created using a 3 μm water-based diamond suspension. Bones were sonicated for 15 sec to remove any residue from the polishing process. In order to expose collagen, bones were demineralized using 0.5 M EDTA at a pH of 8.0 for 15 minutes, and then sonicated for 5 minutes in ultrapure water to liberate unbound mineral crystals and ions from the

surface. This process was repeated a total of three times to create a surface suitable for AFM imaging.

Samples were imaged in air using a Bioscope Catalyst AFM (Bruker, Tucson, AZ). Images were taken in peak force tapping mode using silicon probes on silicon nitride cantilevers (Scanasyst-Fluid+; Bruker, Camarillo, CA) at a scanning rate of 0.5 Hz at 512 lines of resolution for each image. Three to four 25 μm x 25 μm regions were selected along the length of each bone. Areas for fibril analysis were further examined at 10 x 10 μm to search for usable fibril groups. Two to three images at 3.5 x 3.5 μm were acquired at each location, and 10-25 individual fibrils were analyzed. In total, an average of 55 fibrils was measured in each bone. D-spacing of individual collagen fibrils was determined from the power spectrum of a 2D Fast Fourier transform as previously described [11, 13, 51] (SPIP Version 5.1.10, Image Metrology, Denmark). All measurements within a single bone were averaged to produce a single measure from each bone for group comparisons (n = 5 per group). In addition, all individual fibril measurements were used for population comparisons (n = 254-289 per group).

3.3 Raman Spectroscopy

Raman spectroscopy was performed using a LabRAM HR 800 Raman Spectrometer (HORIBA Jobin Yvon, Edison, NJ) connected to a BX41 microscope (Olympus, Tokyo, Japan). A 660 nm laser was focused on the sample surface using a 50X objective to a spot size of ~10 μm. Five locations approximately 1 mm apart along the posterior surface of fresh, unprocessed right femora were placed in a PBS bath with PBS surrounding the bone but not covering the posterior surface. Five 20 sec acquisitions were averaged at each location and baseline corrected to create a single measure at each location (LabSpec 5, HORIBA Jobin Yvon). Using OriginPro 8.6 (OriginLab, Northampton, MA), a single Gaussian peak was fit to the PO_4^{3-} ν1 peak. Areas under the PO_4^{3-} ν1, CO_3^{2-} ν1, Amide III, CH_2 wag, and Amide I peaks were calculated at each

location. All locations were pooled into a single measurement from each bone for group comparisons (n = 5-6 per group).

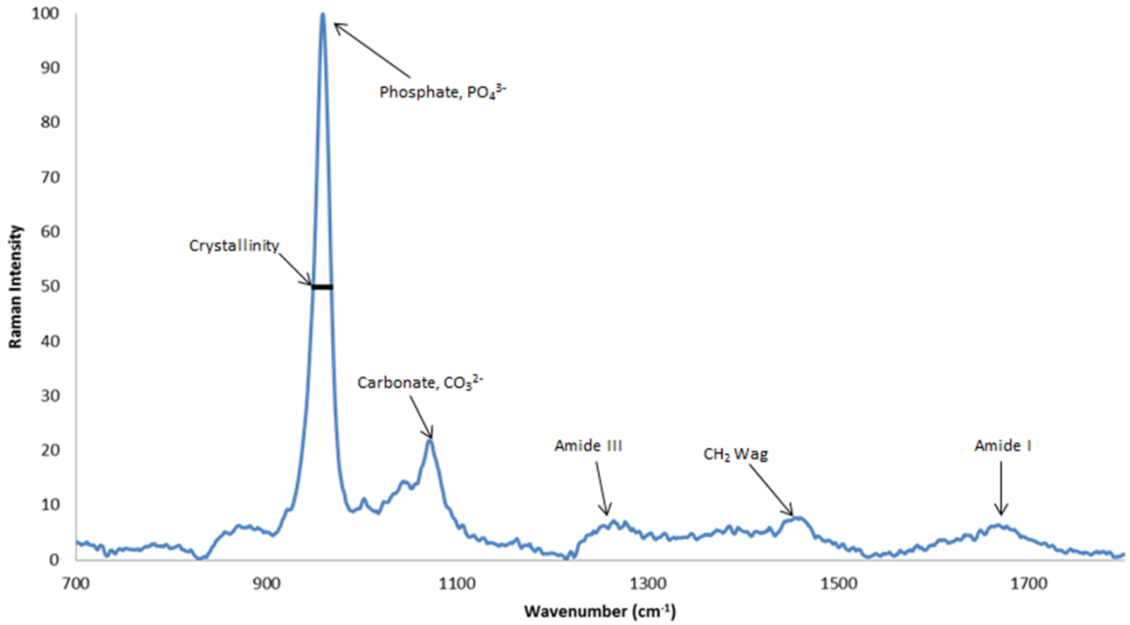

Figure 3.1: A typical Raman spectroscopy spectrum for a single location. Values have been normalized to the maximum value obtained from the scan. Crystallinity is calculated as 1/full width at half maxima (FWHM) of the phosphate peak. Values of PO_4^{3-}, CO_3^{3-}, Amide III, CH_2, and Amide I were calculated via curve fitting of the surrounding Raman spectra.

Type B carbonate substitution levels were calculated from the band area ratio of CO_3^{2-} ν1/ PO_4^{3-} ν1. The degree of matrix mineralization was determined using three distinct band area ratios: PO_4^{3-} ν1/Amide I, PO_4^{3-} ν1/ CH_2 wag, and PO_4^{3-} ν1/Amide III. The ratio of Amide I/Amide III was also calculated to measure changes which may have occurred under the Amide I peak. Crystallinity/maturity was determined by 1/full width at half maxima (FWHM) of the PO_4^{3-} ν1 peak (Figure 3.1).

3.4 Reference Point Indentation

Following Raman spectroscopy, the same femora were tested using a BioDent Reference Point Indentation (RPI) system (Active Life Scientific, Santa Barbara, CA).

Four indentations (BP3 BioDent probe assembly) were made along the length of the posterior surface of each femur, chosen to be in the same region as four of the five Raman measurements (limited to 4 locations due to orientation restrictions with the BioDent sample fixture). Cyclic indentation was performed in load control to 2 N for 5 loading cycles. The indentation probe creates an indent that is approximately 100 μm in diameter [34], allowing for sufficient space between each measurement without interaction with damage induced from previous indents. All bones were hydrated with PBS throughout indentation. Measurements from RPI were calculated using a custom MATLAB script which allows for cycle-by-cycle analysis [52]. Calculated parameters included indentation distance (ID), indentation distance increase (IDI), total indentation distance (TID), creep indentation distance (CID), energy dissipation, and unloading slope, all taken from averaging the values measured in cycles 2-5. Measurements from the four locations in each bone were averaged to produce a single value for each measure in each bone.

3.5 Micro Computed Tomography (μCT)

Ex vivo scans of left femora were performed using a Skyscan 1172 high-resolution μCT (Bruker-MicroCT, Kontich, Belgium). Prior to scans, the overall length of each bone was measured and the bones were inspected for any apparent *in vivo* fractures. Calibration was performed daily using two cylindrical hydroxyapatite phantoms (0.25 and 0.75 g/cm^3 CaHA) and a water sample. Scans were performed at an isotropic voxel size of 11.93 μm resolution (V = 50 kV, I = 167 μA).

Femoral geometric properties were measured from 7 slices centered at the midshaft. Volumetric bone mineral density (BMD) measures were made at five standard sites spaced 2mm apart taken from the posterior quadrant of bone from μCT images to complement measures obtained through Raman spectroscopy. Binary images were then created from these standard sites with a standard threshold set for determining calcified tissue. Standard site geometric information was analyzed using a MATLAB image

analysis processing script [53]. Trabecular analysis in the distal femur was accomplished by setting a cylindrical cross section inside the cortical shell of the bone. A circular face was created just touching the distal growth plate and was then extended to 0.5 mm in the proximal direction to create a volume enclosing the trabecular envelope. A ratio of bone volume to tissue volume (BV/TV) was calculated to assess the trabecular organization within the bone. Additionally, trabeculae in this region were measured for the average thickness of individual struts and the separation between these structures.

3.6 Whole Bone Mechanical Testing

Following μCT, left femora were monotonically tested to failure in displacement control at a loading rate of 0.3 mm/sec in 3-point bending (Test Resources, Model 100R500-12, Shakopee, MN). The apparatus had a support span of 5 mm. Femora were aligned such that the loading point was in contact with the anterior surface of the bone at the mid-diaphysis, testing in the anterior-posterior (AP) direction (posterior surface in tension). Force and displacement were measured during each test at 30 Hz. Following fracture, the fracture location was measured relative to the proximal end of the bone using digital calipers (accurate to 0.01 mm, Marathon, Richmond Hill, Ontario). A subset of geometric properties at the fracture location were obtained from μCT data and were used to convert force and displacement to stress and strain using standard beam bending equations [54].

3.7 Statistical Analysis

With the exception of nanoscale morphology (mean ± standard deviation), all data are presented as mean ± standard error. Statistical analysis was performed using one-Way ANOVA (non-parametric Kruskal-Wallis tests, or two-sample T-tests of unequal variance with Bonferroni correction when appropriate) with pairwise Tukey and Dunn's post hoc tests (SigmaPlot, Jandel Scientific). Measurements lacking homoscedasticity between groups were transformed prior to comparison and then analyzed with

appropriate tests. Kolmogorov-Smirnov tests were performed to assess population differences in collagen fibril D-spacing distributions as previously described [11, 13]. In all cases, a value of $p < 0.05$ was considered significant.

4. RESULTS

4.1 Nanoscale Morphology: Atomic Force Microscopy

To assess the nanoscale morphology of Type I collagen fibrils, the D-periodic spacing of individual fibrils was measured in bone from WT, oim/+ and oim/oim mice. Images were acquired from 3-4 locations in each of 5 bones per animal. 2D Fast Fourier Transforms were performed on 10-25 individual fibrils at each location. Measurements from each bone were averaged to yield the mean fibril spacing for that bone, then the WT, oim/+ and oim/oim values were compared (Figure 4.1). D-spacing in the oim/+ (65.6±0.1 nm) and oim/oim (65.4±0.5 nm) were both significantly lower than WT (66.0±0.2 nm), but were not significantly different from each other.

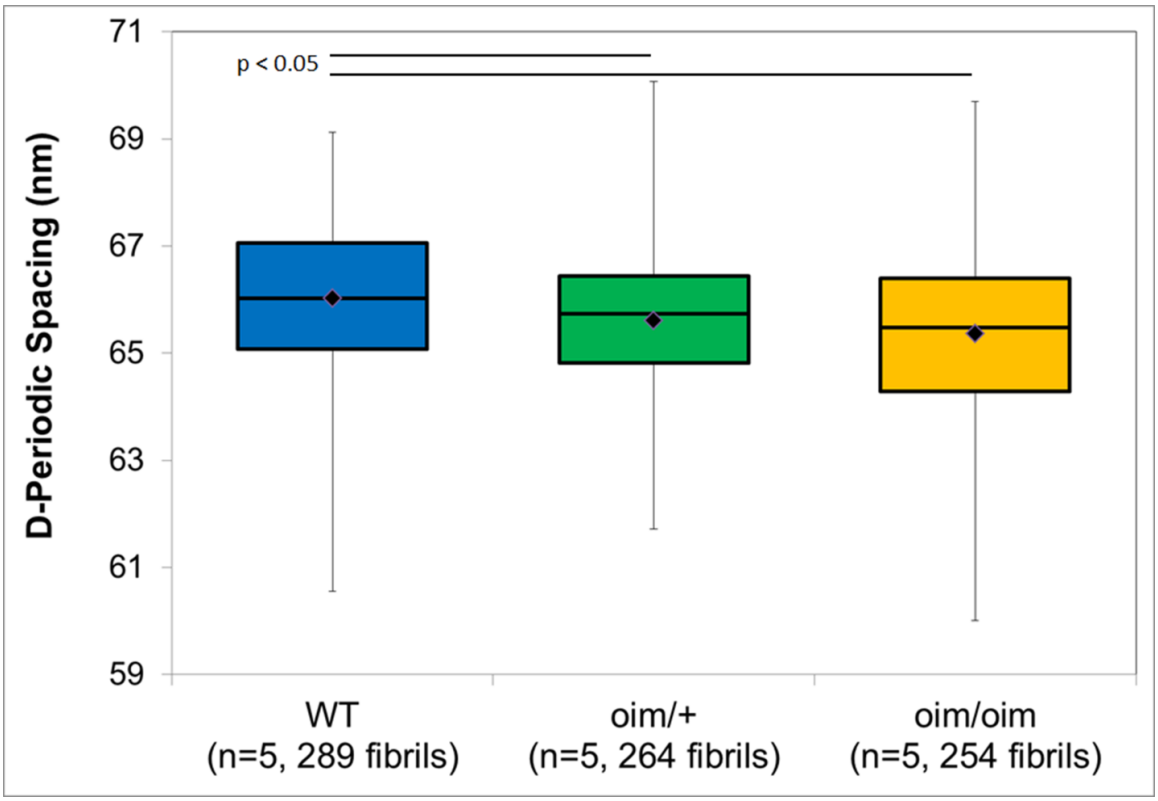

Figure 4.1: Entire distribution of fibrils measured for D-spacing through AFM analysis. While the distribution of all fibers is wide, statistical analysis was done on averages taken for each bone. Non-parametric statistical tests showed WT bones to have higher average fibril D-spacing ($p < 0.05$) than both oim/+ and oim/oim.

Figure 4.2A shows that a distribution of D-period spacings existed in each group. To define a main population of fibrils within each group, fibrils included within the mean ± 1 standard deviation of the entire WT population (289 fibrils) were used. Within this range, 71.3% of WT fibrils, 73.5% of oim/+ fibrils and 63.0% of oim/oim fibrils were found. Below this range, 13.8% of WT fibrils were found in comparison to 18.9% for oim/+ and 28% for oim/oim, indicating that the population distribution in the 2 disease states was shifted downwards versus WT. Kolmogorov-Smirnov tests of fibril populations showed all groups to be distributed differently from one another (Figure 4.2B).

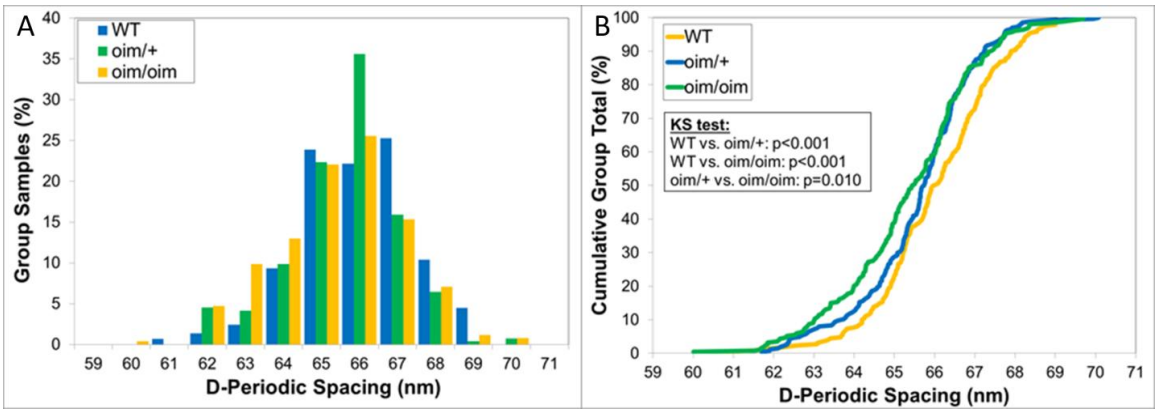

Figure 6.2: Fibril analysis of all fibrils measured. Panel A shows a histogram of fibrils in each group, demonstrating the distributions of all fibrils. Panel B is a cumulative distribution function (CDF) of fibrils depicting differences in the population distributions as indicated by Kolmogorov-Smirnov tests.

4.2 Raman Spectroscopy and Volumetric Bone Mineral Density (vBMD)

The mineral to matrix ratio (MMR) can be measured in several ways, by normalizing the phosphate ν_1 peak to one of several peaks related to collagen (Table 1). For all three measures of MMR used here, the only significant difference was a decrease in MMR Amide I in oim/oim relative to WT. A significant increase in the Amide I:Amide III case in oim/oim versus WT suggests that there is a significant change in the Amide I peak in the oim/oim group. In terms of mineral composition, there was no difference in the carbonate:phosphate ratio between any groups, but there was a significant decrease in crystallinity in oim/oim versus WT and oim/+. Volumetric bone mineral density (vBMD) was also assessed via µCT analysis. Similar to the Raman MMR data, vBMD was lowest in the oim/oim genotype, but only significantly lower than the oim/+ due to the higher error associated with the oim/oim values.

Table 4.1: Assessment of chemical properties obtained via Raman Spectroscopy

	WT(n = 6)	oim/+ (n = 6)	oim/oim (n = 5)
MMR Amide I	2.541±0.125	2.3462±0.128	1.9242±0.056[a]
MMR CH_2	4.344±0.230	4.0673±0.653	3.7616±0.109
MMR Amide III	3.769±0.259	3.7444±0.218	3.4385±0.097
Amide I:Amide III	1.502±0.048	1.6247±0.044	1.7971±0.056[a]
Carbonate:Phosphate	0.503±0.013	0.4997±0.008	0.4990±0.019
Crystallinity	0.054±0.0003	0.0534±0.0001	0.0519±0.0001[a,b]
Volumetric Bone Mineral Density (g/cm^3)*	1.576±0.009	1.591±0.012	1.540±0.024[b]

[a]Significantly different from WT data at $\alpha = 0.05$.
[b]Significantly different from oim/+ data at $\alpha = 0.05$.
* Volumetric bone mineral density (vBMD) measured at five posterior sections along the diaphysis via µCT.

4.3 Reference Point Indentation

Reported values of ID, IDI, CID, and energy dissipation (Table 2) are all measurements related to the accumulation of microdamage induced by cycling the indentation probe [55]. Trends in treatment levels are similar across these variables with increased values in the oim/oim versus WT without an increase in the oim/+ values. With the exception of a significant increase in ID for oim/oim versus both WT and oim/+, no other differences reached statistical significance. Unloading slope is a measure stiffness of a sample, similar to elastic modulus. RPI data suggests no difference in oim/+ versus WT, but a significantly lower value for unloading slope in oim/oim mice versus WT and oim/+.

Table 4.2: Measurements obtained from reference point indentation system

	WT (n = 6)	oim/+ (n = 6)	oim/oim (n = 5)
ID (μm)	9.566±0.307	9.329±0.255	12.528±1.033[a,b]
IDI (μm)	3.912±0.748	3.833±0.280	4.6056±0.911
TID (μm)	31.653±1.070	31.210±1.003	35.291±1.774
CID (μm)	1.184±0.108	1.143±0.068	1.364±0.236
Energy Dissipation (μJ)	4.601±0.480	4.768±0.203	5.283±0.867
Unloading Slope (N/μm)	0.267±0.007	0.271±0.009	0.211±0.009[a,b]

Values presented as the mean ± standard error with all locations in a bone pooled into one measurement

[a]Significantly different from WT data at $\alpha = 0.05$.

[b]Significantly different from oim/+ data at $\alpha = 0.05$.

4.4 Micro Computed Tomography

Severe alterations in bone morphology are typical of the oim model [23]. Figure 4.3 shows schematics of the average cross-section of the femoral mid-diaphysis from each group (data appear in Table 3). Apparent from the images is the significantly reduced total cross sectional area and cortical area in the diseased genotypes. There were also significant decreases in both cortical area and cortical thickness for both disease states. Less apparent is the significantly larger marrow cavity in the WT versus oim/+ and oim/oim. In agreement with other changes, both periosteal and endocortical surface perimeters were decreased in oim/oim relative to WT.

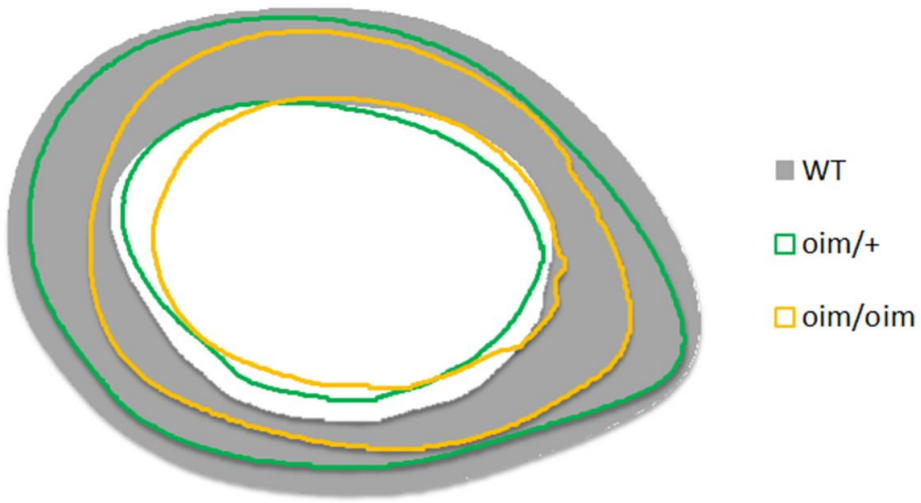

Figure 4.3: Average profiles of oim/+ and oim/oim animal overlaid on the WT average cross-section.

Table 4.3: Standard site measurements of femur cortical geometry

	WT (n = 15)	oim/+ (n = 9)	oim/oim (n = 8-9)
Cross-Sectional Area (mm^2)	1.219±0.019	1.054±0.045[a]	0.745±0.032[a,b]
Cortical Area (mm^2)	1.144±0.036	0.980±0.040[a]	0.632±0.025[a,b]
Marrow Area (mm^2)	0.858±0.023	0.733±0.044[a]	0.733±0.057[a]
Cortical Thickness (mm)	0.274±0.004	0.254±0.009[a]	0.178±0.008[a,b]
Periosteal Surface (mm)	5.900±0.046	5.568±0.087	5.000±0.125[a,b]
Endosteal Surface (mm)	4.100±0.062	3.792±0.103	3.789±0.193[a]

[a]Significantly different from WT data at $\alpha = 0.05$.
[b]Significantly different from oim/+ data at $\alpha = 0.05$.

Trabecular analysis of the distal femur (Figure 4.4) showed a significant decrease in BV/TV with increasing disease severity. Similarly, the average thickness of these trabeculae was significantly decreased in both oim/+ and oim/oim versus WT. The separation between trabeculae was significantly higher in oim/oim versus WT and oim/+, lending to its reduced BV/TV.

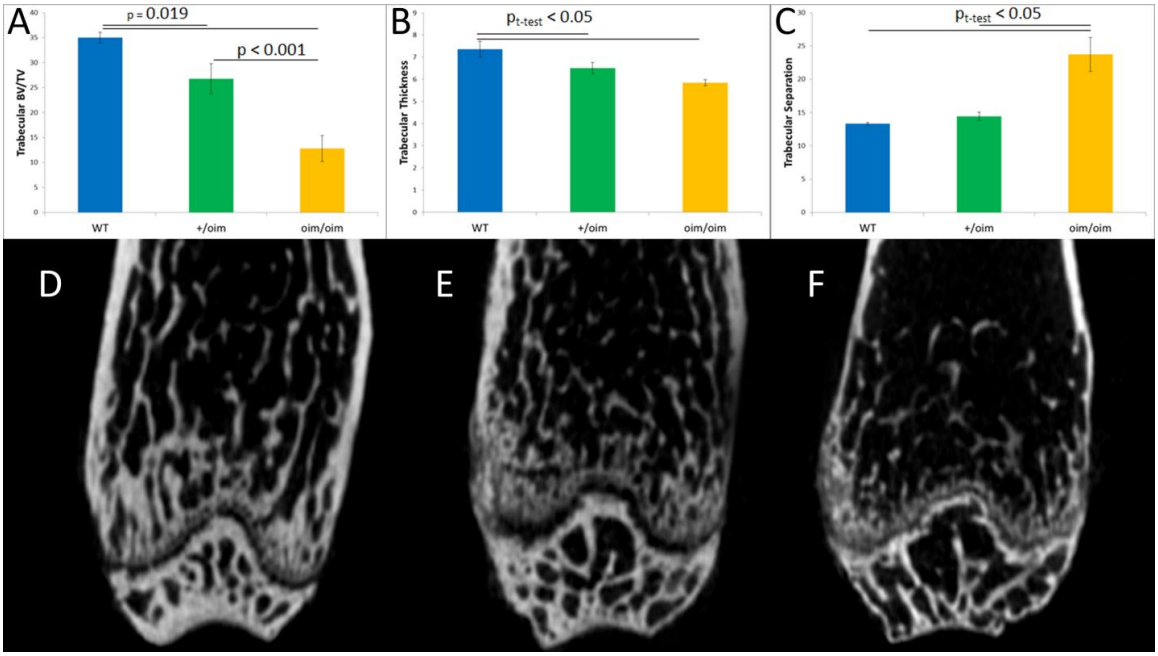

Figure 4.4: Analysis of trabecular structure of distal femur. (A) Trabecular density measure of BV/TV. (B) Average thickness of trabecular webbing. (C) Average separation between individual trabeculae. Data show a significant loss in trabecular amount within the femoral metaphysis. (D-F) Representative sagittal cross-sections of WT, oim/+, and oim/oim femora, showing the degenerated trabecular structure.

4.5 Whole Bone Mechanical Testing – 3 Point Bending

Left femurs underwent three-point bending to failure. Stiffness (Table 4) had a significant trend downwards with disease severity, with oim/oim demonstrating a significant drop from the other two. Yield force was significantly different between all groups, decreasing from WT to oim/+ and further to oim/oim. Ultimate force showed a similar decreasing trend across groups, but only the oim/oim group differed from WT and oim/+. Yield displacement showed an increase in the oim/oim vs oim/+, but not between

other groups. Post-yield displacement had a significant downward trend in the disease states, and both work to yield and failure were significantly reduced in both oim/+ and oim/oim versus WT. Post-yield work showed significant drops with each disease state.

Table 4.4: Additional structural data obtained from three-point bending of left femora.

	WT	oim/+	oim/oim
Stiffness (N/mm)	181.176±7.489	175.280±8.840	69.966±8.402[a,b]
Yield Force (N)	18.539±0.553	14.334±1.329[a]	8.189±0.736[a,b]
Failure Force (N)	24.205±1.216	19.877±8.131	9.382±0.845[a,b]
Yield Displacement (μm)	118.318±4.628	99.057±10.861	136.583±7.558[b]
Postyield Displacement (μm)	391.960±19.821	201.587±24.718[a]	60.254±26.924[a,b]
Yield Work (mJ)	1.088±0.047	0.769±0.123[a]	0.538±0.047[a]
Postyield Work (mJ)	10.090±0.510	3.859±0.5429[a]	0.574±0.297[a,b]

[a]Significantly different from WT data at $\alpha = 0.05$.
[b]Significantly different from oim/+ data at $\alpha = 0.05$.

At the tissue level (Figure 4.5), yield stress was marginally changed amongst groups ($p = 0.069$), but ultimate stress was significantly lower in oim/oim versus both WT and oim/+. Oim/+ bones had lower yield strain versus WT, but the brittle nature of the diseased bones became apparent with the significant decrease in total strain for both oim/+ and oim/oim versus WT, and a drop from oim/+ to oim/oim. Modulus was significantly greater in oim/+ versus both WT and oim/oim but was not significantly different between WT and oim/oim despite a 16% decrease. The oim/oim bones had significantly lower resilience compared to WT, showing a decreased ability of the tissue to elastically store energy. A significant decrease in total toughness between both oim/+ and oim/oim with WT, and a decrease in oim/oim versus oim/+ further indicates a lack of post-yield behavior worsening with disease severity.

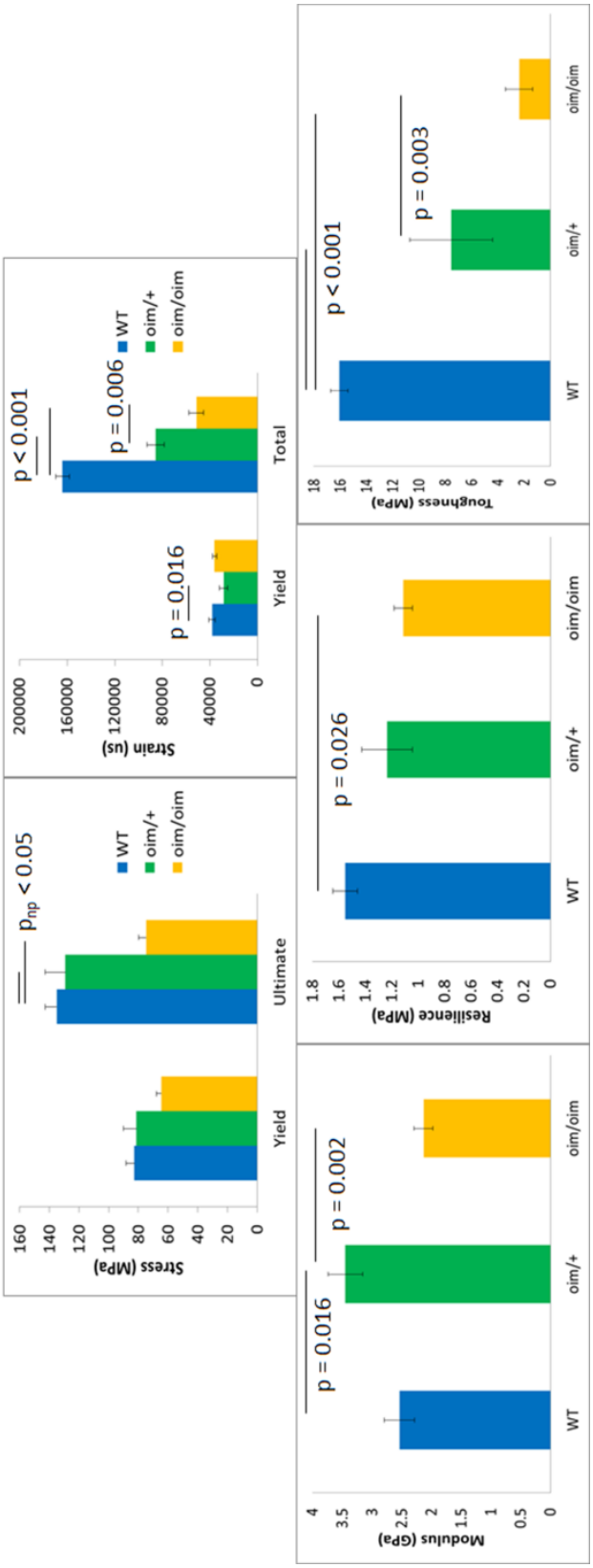

Figure 4.5: Material level properties of left femurs obtained through three-point bending. Post-yield behavior (e.g. Total strain, toughness) points towards a lack of plastic deformation within the oim/+ and oim/oim animals. Structural properties show reduced quality, while tissue level properties point to weaker material. Four-point

5. DISCUSSION

As a genetic disease model that alters collagen formation, analyses in oim bone requires studying nanoscale features to understand how a molecular change in collagen can alter material and structural-level properties in bone and change the development of the skeletal system as a whole. The images in Figures 4.3 and 4.4 illustrate how drastic these changes can be when they propagate up to alter whole bone structure. Ideally, through an assortment of experiments at multiple length scales, it should be possible to find a link between the weakened structure and the base material of bone as fabricated in the body (i.e. collagen fibrils and mineral crystals). Testing at different length scale provides insight into how changes in tropocollagen processing and formation lead to alterations in morphology, tissue chemistry and material mechanical properties. Techniques used in this study maintained hydration within the bone, preventing degradation of mechanical integrity prior to mechanical tests [56]. Additional tests could then be performed on the same samples, as most tests were non-destructive. Damage created by surface indentation tests is limited to local microcracks, allowing for topographic measures of other regions of the bone.

Measurements of D-spacing obtained from AFM measurements provide structural information of collagen at the nanoscale. Mean differences in D-spacing between groups are not typical in disease states as distributions can be wide and sample numbers are typically small [12]. In this study, there was a quantifiable decrease in D-spacing which became more pronounced with disease severity. This difference is likely driven by an increase in the average length of tropocollagen molecules in the homotrimeric state [57] , causing a decreased end-to-end spacing which in turn decreases the D-spacing of the fibril. The decrease noted here is important because this alteration in collagen fibril

structure could have implications on the size of mineral nucleation sites [58], indicating that a change in the organic portion of bone is directly driving alterations in the inorganic phase. The D-spacing distribution is more often used to probe disease-induced differences and has been sensitive enough to detect differences due to osteoporosis in skin [51] and bone [12, 59], and osteogenesis imperfecta in bone and tendon [11, 13]. While a mean difference was present between the oim/oim mice and both other groups, important insight into this difference comes when examining the CDF. Here the oim/oim population shape is similar to WT, but is shifted downward towards lower spacing values. This shift is driven by the fact that 28% of the oim/oim population of fibrils fall outside the mean ±1 standard deviation of the WT group. Interestingly, the lower end of the CDF for the oim/+ group closely follows the WT distribution while at the higher end it is more similar to the oim/oim group. This trend is driven by the jump in fibrils in the oim/+ group with spacings near 66 nm. The difference in distributions indicates that the oim/+ population is an intermediate disease state [27]. Because of the nature of this mutation, all fibrils in the oim/oim group are composed of 100% α1 homotrimers since the animals cannot produce α2 chains. Oim/+ mice have the ability to produce normal α2 chains, meaning that some tropocollagen molecules are α1 homotrimers and some are normal heterotrimers. These are then randomly incorporated into fibrils as they form. The data indicate that some of these fibrils have similarities to normal collagen fibrils from WT mice while others are more characteristic of homotrimers. This observation has important ramifications to the interpretation of mechanical integrity in these bones.

Structural differences between the homotrimer and heterotrimer are likely driving a loss of collagen strength in oim/+ and oim/oim bone. While both α1 and α2 chains possess a Gly-X-Y amino acid repeating structure, the amino acids present in the X-Y positions differ [60]. Hydroxylation of both proline and lysine allows for hydrogen bonding between chains in heterotrimeric molecules [61]. Heterotrimers are aligned in such a way for these bonds to form readily due to the difference in structure between the α1 and α2 molecule primary structure. Additionally, collagen molecules form both inter- and intramolecular cross-links through both enzymatic, and nonenzymatic processes.

Enzymatic cross-linking, catalyzed by lysyl oxidase (LOX), link collagen together through the recognition of unique binding sites on the collagen structure [62]. The difference in the homotrimer structure leads to a different secondary structure, altering binding sites that may lower LOX activity or reduce hydrogen bonding between molecules. Previous studies have shown that there is an increase in the intermolecular distance in homotrimeric structures, causing a reduction in the ability to cross-link in the oim state [43]. Modelling has shown that the amount of cross-linking between collagen molecules plays a key role in the ability to resist deformation [63]. Loss of these key binding structures may reduce the strength of the organic phase in bone.

The interaction of the organic and inorganic phase of bone also determines material properties. Raman spectra of bone generally infer the same base chemical structure given different disease states, but shifts expressed in various peaks give some indication as to how the structure has changed [32]. Differences in genotypes are often seen as alterations within the composition of collagen molecules, resulting in altered material composition of the bone. Altered composition in bone is most apparent through changes in the ratio of organic to inorganic components, or alterations in the crystal size, structure, and perfection. Reduced crystallinity in oim/oim bone has been shown through X-ray diffraction in previous studies [24], and is seen in Raman spectroscopic analyses in the current study. A reduction in crystallinity suggests a defect in the binding and growth of mineral crystals within bone [64]. While vBMD is often a predictor of material modulus [65], the lack of significance in mean vBMD between WT and oim/+ does not explain the significant increase in material modulus in oim/+ bone. Considering typical crystalline materials, like ceramics, crystal size plays a factor in the modulus of the material. Crystal size dictates the level of surface interactions between crystals within the ceramic, i.e. the more surface interactions, the stronger the material [66, 67]. Marginally reduced crystallinity in the oim/+ with vBMD near WT levels may explain the increase of material modulus seen with the mild disease. While the crystallinity is significantly lower in the oim/oim, the significant drop in vBMD indicates fewer, smaller crystals to support the structure and likely led to the drop in modulus in oim/oim versus oim/+.

Whole bone mechanical testing data indicate that oim/+ bones have the highest material modulus. This result may seem counterintuitive, as oim/+ is a milder form of the disease state [27], but as shown above, oim/+ benefits from a higher vBMD and smaller crystals to better resist elastic deformation. Lowered resilience and modulus in the oim/oim indicates degraded elastic behaviour of the material. The brittle nature of the mutated groups can be seen in their lack of post-yield deformation, total deformation, total strain and toughness. These properties are all indicative of the ability of a material and structure to deform and absorb energy without failing and all were decreased in the oim/+ group and further decreased in the oim/oim group versus WT (Figure 4.5). Deficiencies in toughness and postyield displacement indicate that a material and structure is brittle, failing with little plastic deformation. Typically, it is thought that elastic response of bone is driven by mineral while plastic deformation is dominated by the organic phase of the bone [68]. Changes in both preyield and postyield behavior would indicate that the genetic alteration in collagen is influencing both the organic and inorganic phases of the material.

The degraded mineral-matrix structure in oim/oim directly leads to the brittle nature of bone in this animal model which caused significant sample loss here and elsewhere due to premature animal death or *in vivo* fractures [69]. The MMR Amide I appears to indicate a large significant decrease in mineral content for oim/oim bone, but this observation is likely not true. The Amide III band is resistant to alterations from disease states [70], and can be considered constant across all groups here. The significant change noted here in the ratio of Amide I:Amide III suggests a significant alteration in the Amide I band in the two disease states. This observation suggests that the collagen matrix has been altered since the Amide I band is indicative of the secondary structure of collagen [71]. This change in secondary structure can also be detected by the changes in D-spacing distributions noted above. Since the MMR Amide I is the only marker for mineral content that was changed versus WT, this significance is driven by altered collagen, and the other measures of mineralization are more indicative of the actual mineral content. Post-hoc statistical power analysis of Raman MMR measures revealed

slightly lower power levels (P = 0.4-0.5), and these smaller changes may become significantly detectable by increasing Raman sample sizes to 9+ animals to achieve higher power. Importantly, many other studies have used the Amide I band to measure MMR [72, 73]. Data here supports the notion that the MMR Amide I band should be used with caution [70].

Bone as a structure is a complex hierarchy of composite-like mineralized collagen. Organization varies at small length scales due to the directional organization of collagen, but at larger length scales, much is determined by the organization and thickness of trabeculae and cortical bone. Mineral crystallization occurs at a much smaller length scale [74] when compared to the area of material tested using RPI testing or bending [33]. Because of this size difference, it is safe to assume that the same hierarchical level of material is being tested in RPI and bending. It is not surprising that the trend in stiffness measured from micro-scale indentation tests were mirrored by material trends obtained from whole bone mechanical testing. RPI is a new technology that is capable of obtaining clinically-relevant micro-scale mechanical data while minimizing the structural damage induced to the specimen [34, 75]. Because of this, the unloading slope obtained from RPI testing can be used to show differences in bone modulus without inducing major damage to the structure, preserving the remainder of the bone for testing using other techniques. The increasing trend of indentation stiffness was not significant. IDI for oim/oim was 30% higher than WT, but had a considerably higher variance, preventing significance from being reached as well. A lack of significant differences in these measures is likely due to lack of power in the test, which could be remedied by increasing sample sizes in future studies.

According to Wolff's law, bone structures will adapt to the forces that the bone experiences [76]. The material deficiencies of both the organic and inorganic phases that arise from the oim model reduce the ability of bone to resist fracture, resulting in a biological adaptation to alter the bone's structure in an attempt to compensate. Previous studies have shown an increase in bone turnover within these disease states [77]. This

effect is likely a cellular response attempting to remove the malformed collagen matrix. It is possible that the increased cellular response is selectively remodeling areas that are rich in homotrimeric collagen. This observation could account for the recovery of material properties that have been observed over time in the oim/+ animal model [78, 79]. Future studies are planned to look at the progression of the oim/+ and oim/oim phenotypes with aging using the current multiscale approaches. In addition, cellular aspects of these phenotypes will also be interrogated.

6. CONCLUSIONS AND FUTURE DIRECTIONS

Many techniques exist to assess the structural, material and chemical properties of bone. Often, the processing necessary to create samples for these techniques is harsh, limiting the useful and relevant data that can be acquired. Histology and X-ray diffraction both provide valuable information about bone composition. However, histology requires embedding, demineralization, and sectioning, while X-ray diffraction requires the sample to be powdered to assess information about the mineral [80, 81]. Additionally, techniques like transmission electron microscopy or scanning electron microscopy provide equally useful data, but suffer from as harsh sample preparation, including thin sectioning, dehydration, and gold coatings [82, 83]. Assays used in the current study maintained the bone in as close to its native state as possible. Raman Spectroscopy and RPI testing were both done on the surface of unprocessed bones resting in a PBS bath. All mechanical testing was done with continuous hydration of samples. The harshest processing required in the current study was that used to image the bone using AFM. This technique requires a modest amount of demineralization of the bone's surface to expose the underlying collagen. The net result here is that each of the techniques used provide measures as near to a physiological states as possible.

Overall, this study demonstrates how molecular changes to collagen due to a genetic defect can drastically alter properties throughout the tissue hierarchy in both the organic and inorganic portions of bone. Alterations to the collagen triple helix modify the assembly of collagen fibrils. We postulate that the fibrillar defect detected by AFM changes how hydroxyapatite crystals are able to bind and grow in this altered matrix material. Changes in the collagen/mineral composite impact the mechanical properties of

the tissue and ultimately, at the highest levels of organization, the presence of tropocollagen homotrimers creates significantly weaker bone. Future studies will be aimed at assessing nonmineralized tissues to look for similar shifts in periodic D-spacing as well as changes in fibrillar width. These studies will allow for a direct analysis of collagen without the convoluting influence of mineral. Additional studies will be performed to directly assess the molecular cross-linking that occurs in the defective homotrimeric structure.

LIST OF REFERENCES

LIST OF REFERENCES

[1] J. Gong, J. Arnold, and S. Cohn, "Composition of trabecular and cortical bone," *The Anatomical Record,* vol. 149, pp. 325-331, 1964.

[2] D. B. Burr and M. R. Allen, *Basic and Applied Bone Biology*: Academic Press, 2013.

[3] D. Vashishth, O. Verborgt, G. Divine, M. Schaffler, and D. Fyhrie, "Decline in osteocyte lacunar density in human cortical bone is associated with accumulation of microcracks with age," *Bone,* vol. 26, pp. 375-380, 2000.

[4] S. Qiu, D. Rao, S. Palnitkar, and A. Parfitt, "Age and distance from the surface but not menopause reduce osteocyte density in human cancellous bone," *Bone,* vol. 31, pp. 313-318, 2002.

[5] M. Mullender, D. Van der Meer, R. Huiskes, and P. Lips, "Osteocyte density changes in aging and osteoporosis," *Bone,* vol. 18, pp. 109-113, 1996.

[6] A. Boskey, "Bone mineral crystal size," *Osteoporosis international,* vol. 14, pp. S16-S21, 2003.

[7] G. A. Di Lullo, S. M. Sweeney, J. Körkkö, L. Ala-Kokko, and J. D. San Antonio, "Mapping the ligand-binding sites and disease-associated mutations on the most abundant protein in the human, type I collagen," *Journal of Biological Chemistry,* vol. 277, pp. 4223-4231, 2002.

[8] J. Prockop, "Collagens: molecular biology, diseases, and potentials for therapy," *Annual review of biochemistry,* vol. 64, pp. 403-434, 1995.

[9] A. Rich and F. Crick, "The structure of collagen," 1955.

[10] S. Tomlin and C. Worthington, "Low-angle X-ray diffraction patterns of collagen," *Proceedings of the Royal Society of London. Series A. Mathematical and Physical Sciences,* vol. 235, pp. 189-201, 1956.

[11] A. Kemp, C. Harding, W. A. Cabral, J. C. Marini, and J. M. Wallace, "Effects of tissue hydration on nanoscale structural morphology and mechanics of individual Type I collagen fibrils in the Brtl mouse model of Osteogenesis Imperfecta," *Journal of structural biology*, 2012.

[12] J. M. Wallace, B. Erickson, C. M. Les, B. G. Orr, and M. M. Banaszak Holl, "Distribution of type I collagen morphologies in bone: Relation to estrogen depletion," *Bone*, vol. 46, pp. 1349-1354, 2010.

[13] J. M. Wallace, B. G. Orr, J. C. Marini, and M. M. B. Holl, "Nanoscale morphology of Type I collagen is altered in the Brtl mouse model of Osteogenesis Imperfecta," *Journal of structural biology*, vol. 173, pp. 146-152, 2011.

[14] A. Hodge and J. Petruska, "Recent studies with the electron microscope on ordered aggregates of the tropocollagen molecule," *Aspects of protein structure*, pp. 289-300, 1963.

[15] W. Traub, T. Arad, and S. Weiner, "Origin of mineral crystal growth in collagen fibrils," *Matrix*, vol. 12, pp. 251-255, 1992.

[16] J. P. Orgel, T. C. Irving, A. Miller, and T. J. Wess, "Microfibrillar structure of type I collagen in situ," *Proceedings of the National Academy of Sciences*, vol. 103, pp. 9001-9005, 2006.

[17] W. Landis, M. Song, A. Leith, L. McEwen, and B. McEwen, "Mineral and organic matrix interaction in normally calcifying tendon visualized in three dimensions by high-voltage electron microscopic tomography and graphic image reconstruction," *Journal of structural biology*, vol. 110, pp. 39-54, 1993.

[18] D. Urry, "Neutral sites for calcium ion binding to elastin and collagen: a charge neutralization theory for calcification and its relationship to atherosclerosis," *Proceedings of the National Academy of Sciences*, vol. 68, pp. 810-814, 1971.

[19] J. C. Marini, A. Forlino, W. A. Cabral, A. M. Barnes, J. D. San Antonio, S. Milgrom, *et al.*, "Consortium for osteogenesis imperfecta mutations in the helical domain of type I collagen: regions rich in lethal mutations align with collagen binding sites for integrins and proteoglycans," *Human mutation*, vol. 28, pp. 209-221, 2007.

[20] D. O. Sillence, A. Senn, and D. Danks, "Genetic heterogeneity in osteogenesis imperfecta," *Journal of medical genetics*, vol. 16, pp. 101-116, 1979.

[21] K. M. Kozloff, A. Carden, C. Bergwitz, A. Forlino, T. E. Uveges, M. D. Morris, *et al.*, "Brittle IV mouse model for osteogenesis imperfecta IV demonstrates postpubertal adaptations to improve whole bone strength," *Journal of bone and mineral research,* vol. 19, pp. 614-622, 2004.

[22] J. Bonadio, T. L. Saunders, E. Tsai, S. A. Goldstein, J. Morris-Wiman, L. Brinkley, *et al.*, "Transgenic mouse model of the mild dominant form of osteogenesis imperfecta," *Proceedings of the National Academy of Sciences,* vol. 87, pp. 7145-7149, 1990.

[23] S. D. Chipman, H. O. Sweet, D. J. McBride, M. T. Davisson, S. C. Marks, A. R. Shuldiner, *et al.*, "Defective pro alpha 2 (I) collagen synthesis in a recessive mutation in mice: a model of human osteogenesis imperfecta," *Proceedings of the National Academy of Sciences,* vol. 90, pp. 1701-1705, 1993.

[24] N. P. Camacho, L. Hou, T. R. Toledano, W. A. Ilg, C. F. Brayton, C. L. Raggio, *et al.*, "The material basis for reduced mechanical properties in oim mice bones," *Journal of Bone and Mineral Research,* vol. 14, pp. 264-272, 1999.

[25] D. J. McBride, V. Choe, J. R. Shapiro, and B. Brodsky, "Altered collagen structure in mouse tail tendon lacking the α2 (I) chain," *Journal of molecular biology,* vol. 270, pp. 275-284, 1997.

[26] S.-W. Chang, S. J. Shefelbine, and M. J. Buehler, "Structural and mechanical differences between collagen homo-and heterotrimers: Relevance for the molecular origin of brittle bone disease," *Biophysical Journal,* vol. 102, pp. 640-648, 2012.

[27] J. Saban, M. Zussman, R. Havey, A. Patwardhan, G. Schneider, and D. King, "Heterozygous oim mice exhibit a mild form of osteogenesis imperfecta," *Bone,* vol. 19, pp. 575-579, 1996.

[28] G. E. Lopez Franco, A. Huang, N. Pleshko Camacho, and R. D. Blank, "Dental phenotype of the col1a2 oim mutation: DI is present in both homozygotes and heterozygotes," *Bone,* vol. 36, pp. 1039-1046, 2005.

[29] A. G. Vouyouka, B. J. Pfeiffer, T. K. Liem, T. A. Taylor, J. Mudaliar, and C. L. Phillips, "The role of type I collagen in aortic wall strength with a homotrimeric [α1 (I)] 3 collagen mouse model," *Journal of vascular surgery,* vol. 33, pp. 1263-1270, 2001.

[30] J. A. Timlin, A. Carden, and M. D. Morris, "Chemical microstructure of cortical bone probed by Raman transects," *Applied Spectroscopy,* vol. 53, pp. 1429-1435, 1999.

[31] R. Smith and I. Rehman, "Fourier transform Raman spectroscopic studies of human bone," *Journal of Materials Science: Materials in Medicine,* vol. 5, pp. 775-778, 1994.

[32] J. Ager, R. K. Nalla, K. L. Breeden, and R. O. Ritchie, "Deep-ultraviolet Raman spectroscopy study of the effect of aging on human cortical bone," *Journal of biomedical optics,* vol. 10, pp. 034012-0340128, 2005.

[33] M. A. Gallant, D. M. Brown, J. M. Organ, M. R. Allen, and D. B. Burr, "Reference-point indentation correlates with bone toughness assessed using whole-bone traditional mechanical testing," *Bone,* 2012.

[34] A. Diez-Perez, R. Güerri, X. Nogues, E. Cáceres, M. J. Peña, L. Mellibovsky, *et al.*, "Microindentation for in vivo measurement of bone tissue mechanical properties in humans," *Journal of Bone and Mineral Research,* vol. 25, pp. 1877-1885, 2010.

[35] S. Weiner and H. D. Wagner, "The material bone: structure-mechanical function relations," *Annual Review of Materials Science,* vol. 28, pp. 271-298, 1998.

[36] S. A. Goldstein, "The mechanical properties of trabecular bone: dependence on anatomic location and function," *Journal of biomechanics,* vol. 20, pp. 1055-1061, 1987.

[37] C. M. Bagi, N. Hanson, C. Andresen, R. Pero, R. Lariviere, C. H. Turner, *et al.*, "The use of micro-CT to evaluate cortical bone geometry and strength in nude rats: correlation with mechanical testing, pQCT and DXA," *Bone,* vol. 38, pp. 136-144, 2006.

[38] B. Wopenka and J. D. Pasteris, "A mineralogical perspective on the apatite in bone," *Materials Science and Engineering: C,* vol. 25, pp. 131-143, 2005.

[39] M. Giraud-Guille, "Twisted plywood architecture of collagen fibrils in human compact bone osteons," *Calcified tissue international,* vol. 42, pp. 167-180, 1988.

[40] R. E. Neuman and M. A. Logan, "The determination of collagen and elastin in tissues," *Journal of Biological Chemistry,* vol. 186, pp. 549-556, 1950.

[41] J. M. Wallace, Q. Chen, M. Fang, B. Erickson, B. G. Orr, and M. M. Banaszak Holl, "Type I collagen exists as a distribution of nanoscale morphologies in teeth, bones, and tendons," *Langmuir,* vol. 26, pp. 7349-7354, 2010.

[42] F. Rauch and F. H. Glorieux, "Osteogenesis imperfecta," *The Lancet,* vol. 363, pp. 1377-1385, 2004.

[43] C. A. Miles, T. J. Sims, N. P. Camacho, and A. J. Bailey, "The Role of the α2 Chain in the Stabilization of the Collagen Type I Heterotrimer: A Study of the Type I Homotrimer in oim Mouse Tissues," *Journal of molecular biology,* vol. 321, pp. 797-805, 2002.

[44] X. N. Dong, M. Zoghi, Q. Ran, and X. Wang, "Collagen mutation causes changes of the microdamage morphology in bone of an OI mouse model," *Bone,* vol. 47, pp. 1071-1075, 2010.

[45] S. Rao, K. Evans, A. Oberbauer, and R. Martin, "Bisphosphonate treatment in the oim mouse model alters bone modeling during growth," *Journal of biomechanics,* vol. 41, pp. 3371-3376, 2008.

[46] D.J. McBride, J. Shapiro, and M. Dunn, "Bone geometry and strength measurements in aging mice with the oim mutation," *Calcified tissue international,* vol. 62, pp. 172-176, 1998.

[47] E. M. Horwitz, D. J. Prockop, L. A. Fitzpatrick, W. W. Koo, P. L. Gordon, M. Neel, *et al.,* "Transplantability and therapeutic effects of bone marrow-derived mesenchymal cells in children with osteogenesis imperfecta," *Nature medicine,* vol. 5, pp. 309-313, 1999.

[48] F. H. Glorieux, N. J. Bishop, H. Plotkin, G. Chabot, G. Lanoue, and R. Travers, "Cyclic administration of pamidronate in children with severe osteogenesis imperfecta," *New England Journal of Medicine,* vol. 339, pp. 947-952, 1998.

[49] F. Rauch, R. Travers, H. Plotkin, and F. H. Glorieux, "The effects of intravenous pamidronate on the bone tissue of children and adolescents with osteogenesis imperfecta," *Journal of Clinical Investigation,* vol. 110, pp. 1293-1299, 2002.

[50] E. Åström and S. Söderhäll, "Beneficial effect of bisphosphonate during five years of treatment of severe osteogenesis imperfecta," *Acta Paediatrica,* vol. 87, pp. 64-68, 1998.

[51] B. Erickson, M. Fang, J. M. Wallace, B. G. Orr, C. M. Les, and M. M. Banaszak Holl, "Nanoscale structure of type I collagen fibrils: Quantitative measurement of D-spacing," *Biotechnology Journal,* vol. 8, pp. 117-126, 2013.

[52] G. M. Aref, J.M. Wallace, C.L. Newman, D.M. Brown, D.B. Burr, M.R. Allen, "In vivo reference point indentation reveals positive effects of raloxifene on mechanical properties following six months of treatment in skeletally mature beagle dogs," *Bone,* In Press, 2013.

[53] J. M. Wallace, R. M. Rajachar, X.-D. Chen, S. Shi, M. R. Allen, S. A. Bloomfield, *et al.*, "The mechanical phenotype of biglycan-deficient mice is bone- and gender-specific," *Bone,* vol. 39, pp. 106-116, 2006.

[54] C. H. Turner and D. B. Burr, "Basic biomechanical measurements of bone: a tutorial," *Bone,* vol. 14, pp. 595-608, 1993.

[55] Y. Y. Ding, T. Adschiri, G. A. Williams, K. E. Callon, M. Watson, D. Naot, *et al.*, "Validation of BioDent TDI as a New Clinical Diagnostic Method," *Advanced Materials Research,* vol. 275, pp. 151-154, 2011.

[56] W. T. Dempster and R. T. Liddicoat, "Compact bone as a non-isotropic material," *American Journal of Anatomy,* vol. 91, pp. 331-362, 1952.

[57] D. J. Hulmes, A. Miller, S. W. White, and B. B. Doyle, "Interpretation of the meridional X-ray diffraction pattern from collagen fibres in terms of the known amino acid sequence," *Journal of molecular biology,* vol. 110, pp. 643-666, 1977.

[58] S. F. Jackson, "The fine structure of developing bone in the embryonic fowl," *Proceedings of the Royal Society of London. Series B, Biological Sciences,* pp. 270-280, 1957.

[59] S.J. Warden, A.L. Hurd, J.M. Wallace, M.A. Gallant, J.S. Richard, L.A. George, "Elevated Mechanical Loading When Young Provides Lifelong Benefits to Cortical Bone Properties in Female Rats Independent of Surgically-Induced Menopause," *Endocrinology,* 2013.

[60] R. L. Strausberg, E. A. Feingold, L. H. Grouse, J. G. Derge, R. D. Klausner, F. S. Collins, *et al.*, "Generation and initial analysis of more than 15,000 full-length human and mouse cDNA sequences," *Proceedings of the National Academy of Sciences of the United States of America,* vol. 99, p. 16899, 2002.

[61] S. Viguet-Carrin, P. Garnero, and P. Delmas, "The role of collagen in bone strength," *Osteoporosis International,* vol. 17, pp. 319-336, 2006.

[62] R. C. Siegel, "Biosynthesis of collagen crosslinks: increased activity of purified lysyl oxidase with reconstituted collagen fibrils," *Proceedings of the National Academy of Sciences,* vol. 71, pp. 4826-4830, 1974.

[63] M. J. Buehler, "Nanomechanics of collagen fibrils under varying cross-link densities: atomistic and continuum studies," *Journal of the Mechanical Behavior of Biomedical Materials,* vol. 1, pp. 59-67, 2008.

[64] N. Kavukcuoglu, P. Patterson-Buckendahl, and A. Mann, "Effect of osteocalcin deficiency on the nanomechanics and chemistry of mouse bones," *Journal of the mechanical behavior of biomedical materials,* vol. 2, pp. 348-354, 2009.

[65] T. M. Link, S. Majumdar, J. C. Lin, D. Newitt, P. Augat, X. Ouyang, *et al.*, "A comparative study of trabecular bone properties in the spine and femur using high resolution MRI and CT," *Journal of Bone and Mineral Research,* vol. 13, pp. 122-132, 1998.

[66] R. Raj and M. Ashby, "On grain boundary sliding and diffusional creep," *Metallurgical transactions,* vol. 2, pp. 1113-1127, 1971.

[67] Y. Zhou, U. Erb, K. Aust, and G. Palumbo, "The effects of triple junctions and grain boundaries on hardness and Young's modulus in nanostructured Ni–P," *Scripta Materialia,* vol. 48, pp. 825-830, 2003.

[68] A. H. Burstein, J. Zika, K. Heiple, and L. Klein, "Contribution of collagen and mineral to the elastic-plastic properties of bone," *The Journal of bone and joint surgery. American volume,* vol. 57, p. 956, 1975.

[69] X. Yao, S. M. Carleton, A. D. Kettle, J. Melander, C. L. Phillips, and Y. Wang, "Gender-Dependence of Bone Structure and Properties in Adult Osteogenesis Imperfecta Murine Model," *Annals of Biomedical Engineering,* pp. 1-11, 2013.

[70] J. S. Nyman, A. J. Makowski, C. A. Patil, T. P. Masui, E. C. O'Quinn, X. Bi, *et al.*, "Measuring differences in compositional properties of bone tissue by confocal Raman spectroscopy," *Calcified tissue international,* vol. 89, pp. 111-122, 2011.

[71] R. W. Williams, "Estimation of protein secondary structure from the laser Raman amide I spectrum," *Journal of molecular biology,* vol. 166, pp. 581-603, 1983.

[72] M. G. Orkoula, M. Z. Vardaki, and C. G. Kontoyannis, "Study of bone matrix changes induced by osteoporosis in rat tibia using Raman spectroscopy," *Vibrational Spectroscopy,* 2012.

[73] M. Raghavan, N. D. Sahar, D. H. Kohn, and M. D. Morris, "Age-specific profiles of tissue-level composition and mechanical properties in murine cortical bone," *Bone,* vol. 50, pp. 942-953, 2012.

[74] S. Weiner and W. Traub, "Bone structure: from angstroms to microns," *The FASEB journal,* vol. 6, pp. 879-885, 1992.

[75] R. C. Güerri-Fernández, X. Nogués, J. M. Quesada Gómez, E. Torres del Pliego, L. Puig, N. García-Giralt, *et al.*, "Microindentation for in vivo measurement of bone tissue material properties in atypical femoral fracture patients and controls," *Journal of Bone and Mineral Research*, vol. 28, pp. 162-168, 2013.

[76] S. Cowin, "Wolff's law of trabecular architecture at remodeling equilibrium," *Journal of biomechanical engineering*, vol. 108, p. 83, 1986.

[77] I. Kalajzic, J. Terzic, Z. Rumboldt, K. Mack, A. Naprta, F. Ledgard, *et al.*, "Osteoblastic response to the defective matrix in the osteogenesis imperfecta murine (oim) mouse," *Endocrinology*, vol. 143, pp. 1594-1601, 2002.

[78] C. Phillips, D. Bradley, C. Schlotzhauer, M. Bergfeld, C. Libreros-Minotta, L. Gawenis, *et al.*, " Oim mice exhibit altered femur and incisor mineral composition and decreased bone mineral density," *Bone*, vol. 27, pp. 219-226, 2000.

[79] B. Grabner, W. Landis, P. Roschger, S. Rinnerthaler, H. Peterlik, K. Klaushofer, *et al.*, "Age-and genotype-dependence of bone material properties in the osteogenesis imperfecta murine model (oim)," *Bone*, vol. 29, pp. 453-457, 2001.

[80] B. E. Warren, *X-ray Diffraction*: Courier Dover Publications, 1969.

[81] W. Bloom and D. W. Fawcett, *A textbook of histology*: Saunders, 1975.

[82] D. B. Williams and C. B. Carter, *The Transmission Electron Microscope*: Springer, 1996.

[83] J. Goldstein, D. E. Newbury, D. C. Joy, C. E. Lyman, P. Echlin, E. Lifshin, *et al.*, *Scanning electron microscopy and X-ray microanalysis*: Springer, 2003.